FRACTURE OF CRACKED PLATES UNDER PLANE STRESS

By J. C. Newman, Jr.

NASA Langley Research Center
Langley Station, Hampton, Va.

Presented at the National Symposium on Fracture Mechanics

Bethlehem, Pennsylvania
June 19-21, 1967

FRACTURE OF CRACKED PLATES UNDER PLANE STRESS

By J. C. Newman, Jr.
Langley Research Center

ABSTRACT

Dugdale's model for static yielding at the tip of a crack is extended to include the influence of the stress-strain curve on the plastic-zone size and subsequently on the fracture strength of the plate. The internal stresses acting on the boundary of an assumed extension of the crack line to the end of the plastic zone are expressed as a function of strain hardening, strain rate, and the state of stress. Thus, the plastic-zone size and the crack boundary displacements are calculated as a function of these factors for the plane stress condition. From these considerations, a fracture toughness equation which accounts for plasticity is derived for the uniformly loaded plate.

Residual static strength tests on cracked plates for several aluminum alloys and steels at room temperature having widths ranging from 3 to 48 inches are analyzed according to the proposed model. The gross stress predictions computed by using the modified Dugdale model are compared with the predictions computed by the ASTM method and Notch Strength Analysis method in tables II to VI. The proposed method gave predictions that were more consistent with the test data.

SYMBOLS

A	material constant
a	half-length of crack, in.
a_c	critical half-length of crack, in.
a_o	initial half-length of crack, in.
$\dot{a}$	crack velocity, in/sec
B	material constant
b	half-width of plate, in.
c	length of plastic zone plus half-length of crack, in.
C	coefficient for slow crack extension
C_m	crack sensitivity for the Notch Strength Analysis method, $in.^{-1/2}$

D	material density, slugs/in.^{3}
d	distance from crack tip to point of interest in plastic zone, in.
E	Young's modulus, psi
K_c	fracture toughness for the ASTM method, lbf-(in.)$^{-3/2}$
$\bar{k}_c$	fracture toughness for the modified Dugdale model, lbf-(in.)$^{-3/2}$
m	strain-rate exponent
m_o	strain-rate exponent at the yield strain
n	strain-hardening exponent
n_o	strain-hardening exponent at a strain rate of 0.005 per sec
p_o	exponent for the influence of strain rate on strain hardening
r	notch root radius, in.
S	gross stress applied to the plate, psi
$\dot{S}$	gross stress rate applied to the plate, psi/sec
S_{G_c}	maximum gross stress at failure, psi
S_{N_c}	net section stress based on critical crack length, psi
S_{N_o}	net section stress based on initial crack length, psi
T	temperature, ^oF
t	thickness, in.
v_a	displacement at the crack tip measured in the y-axis direction, in.
w	width of plate, in.
Z	exponent for slow crack extension
α_p	elastic-plastic width correction factor
γ	ratio of transverse to longitudinal stress in plastic zone
$\tilde{\epsilon}$	true strain
ϵ_y	engineering yield strain

ϵ_{y_o}	engineering yield strain at a strain rate of 0.005 per sec
$\dot{\epsilon}$	strain rate, per sec
$\dot{\epsilon}_o$	strain rate of 0.005 per sec
ρ	plastic-zone size, in.
$\dot{\rho}$	rate of change of plastic-zone size, in/sec
$\bar{\sigma}$	true stress, psi
σ_u	engineering ultimate strength, psi
σ_{u_o}	engineering ultimate strength at a strain rate of 0.005 per sec, psi
σ_y	engineering yield stress (0.2-percent offset), psi
σ_{y_o}	engineering yield stress (0.2-percent offset) at a strain rate of 0.005 per sec, psi
ξ	distance from end of plastic zone to point of interest within the zone, in.

INTRODUCTION

Many aspects of material behavior contribute to the catastrophic growth of cracks in plates under monotonically increasing load. A general view concerning the behavior of material at the leading edge of a crack is that plastic flow and subsequent fracture of the material is influenced by factors such as strain hardening, strain rate, the state of stress, and temperature. Therefore, it becomes apparent that further progress in the field of fracture mechanics demands appropriate elastic-plastic solutions that can describe what occurs in the plastic zone as a function of loads and mechanical properties. The elastic-plastic problem has been considered by Swedlow (ref. 1) and several others (refs. 2 and 3). While these analyses have produced information to indicate the role of plasticity in notched or cracked plates, they have yet to produce a criterion for fracture useful to the designer.

In the present paper, Dugdale's model (ref. 4) for static yielding at the tip of a crack is extended to include the influence of the stress-strain curve on the plastic-zone size and subsequently on the fracture strength of the plate. In modifying the model, the stresses in the plastic zone are expressed as a function of the plastic flow properties. These properties are influenced by factors such as the state of stress (e.g., plane stress or plane strain), strain hardening, strain rate, and the test temperature. In this paper, only the case of plane stress at room temperature is considered. From these considerations,

a fracture toughness equation, similar to that obtained by Irwin (ref. 5), is derived to account for plasticity. This equation reduces to the linear-elastic stress-intensity factor when the plastic-zone size becomes zero.

Residual static strength tests on cracked plates for several aluminum alloys and steels of various widths at room temperature are analyzed according to the proposed model. The gross stress predictions computed by using the modified Dugdale model are compared with the predictions computed by the ASTM method (ref. 5) and the Notch Strength Analysis method (refs. 6 and 7).

DUGDALE MODEL

The Dugdale model has a wedge-shaped plastic zone ahead of the crack tip as shown in figure 1(a). The plastic zone may be replaced by an internal-stress distribution acting on the boundary of the plastic zone as shown in figure 1(b). (Barenblatt (ref. 8) has used a similar approach to study the cohesive strength of brittle materials.) The model is based on the following assumptions:

(1) The material in the plastic zone is under a uniform stress equal to the yield stress σ_y of the material.

(2) The material outside the extended crack $2c$ is elastic.

(3) The plastic-zone size ρ is such that no stress singularity appears at the ends of the extended crack.

From these assumptions, Dugdale obtained the following solution for the plastic-zone size:

$$\rho = a\left(\sec \frac{\pi S}{2\sigma_y} - 1\right) \tag{1}$$

As a matter of interest, a mathematical method developed by Muskhelishvili was used by Goodier and Field (ref. 9) to solve for the crack boundary displacements for the Dugdale model. The displacement at the tip of the actual crack ($x = a$) in the model is

$$v_a = \frac{4\sigma_y a}{\pi E} \ln \sec \frac{\pi S}{2\sigma_y} \tag{2}$$

In cracked plate tests on steels, Dugdale (ref. 4), Rosenfield, Dai and Hahn (ref. 10), and Forman (ref. 11) have observed a zone of plastically deformed material consistent in shape and magnitude with the wedge-shaped zone assumed in the Dugdale model. On the other hand, Ault and Spretnak (ref. 2) with sharp notches in molybdenum, and Gerberich (ref. 12) with cracks in several aluminum alloys have observed plastic zones which differ considerably from the wedge-shaped zone. Analytical works of Stimpson and Eaton (ref. 3) and

Swedlow (ref. 1) indicate plastic zones more nearly in agreement with the latter observations (refs. 2 and 12). However, the simplicity of the Dugdale model allows a mathematical treatment of plastic yielding at the crack tip. One of the assumptions of the Dugdale model is that the internal-stress distribution in the plastic zone is constant. In actuality, this stress distribution is not constant and varies with the material properties.

MODIFIED DUGDALE MODEL

In this paper, Dugdale's model for static yielding at the tip of a crack is extended to include the influence of the stress-strain curve on the plastic-zone size and subsequently on the fracture strength of the plate. In an actual case of a crack propagating in a plate, the plastic-zone size is controlled by the flow characteristics of the material. In this paper the dynamic effects are accounted for by describing the dynamic stress-strain behavior. The inertial effects are negligible because the gross stress rates and crack velocities of interest are relatively low. Thus, the modification of the model consists of describing the internal-stress distribution in the plastic zone as a function of strain hardening, strain rate, and the state of stress. In order to achieve this goal, several basic assumptions have to be made regarding the distribution of strains and the state of stress in the plastic zone.

Strain

The equation for the true strains in the plastic zone is assumed to be of the form

$$\bar{\epsilon} = \epsilon_y \left(\frac{\rho}{d}\right)^{\frac{1}{n+1}} \tag{3}$$

where the true yield strain and the engineering yield strain are assumed to be equal. Equation (3) is the tensile analog of the equation derived in reference 13 for the Mode III (longitudinal shear) elastic-plastic behavior.

Strain Rate

The strain rates are calculated directly from the strain expression (eq. (3)) by differentiating with respect to time. If the yield strain and strain-hardening exponent are assumed constant for a particular point of interest ($x = a + d$) in the plastic zone, see figure 2, the strain rate is given by

$$\dot{\bar{\epsilon}} = \frac{\epsilon_y}{n+1}\left(\frac{\rho}{d}\right)^{\frac{1}{n+1}} \frac{\dot{\rho}}{\rho} \tag{4}$$

where $\dot{\rho}$ is the rate of change in the plastic-zone size. The variation in the yield strain and the strain-hardening exponent with strain rate are accounted for in that the values of yield strain and strain-hardening exponent vary for different point of interest in the plastic zone. In order to determine ρ, the equation for the plastic-zone size is assumed to have the form

$$\rho = Aa\left(\sec \frac{\pi S}{2B\sigma_{y_o}} - 1\right) \tag{5}$$

where the constants A and B are determined from the analysis by an iteration procedure, see appendix B. This form is chosen for convenience in describing the plastic-zone size. The constants A and B account for the varying internal-stress distribution in the plastic zone. When the internal-stress distribution is constant and equal to the yield stress, the values of A and B are unity and equation (5) reduces to equation (1). By differentiating equation (5) with respect to time, the rate of change in the plastic-zone size normalized with crack length is given by

$$\frac{\dot{\rho}}{a} = \frac{\rho}{a}\left(\frac{\dot{a}}{a}\right) + \frac{\pi A}{2B}\left(\frac{\rho}{Aa} + 1\right)\sqrt{\left(\frac{\rho}{Aa}\right)^2 + 2\,\frac{\rho}{Aa}}\left(\frac{\dot{S}}{\sigma_y}\right) \tag{6}$$

where $\dot{a}$ is the crack velocity and $\dot{S}$ is the gross stress rate.

State of Stress

The state of stress in the plastic zone is determined as follows. The crack tip is visualized as having a notch root radius r equal to the crack-tip displacement v_a. The crack-tip displacement is calculated from equation (B1) (see appendix B). The notch root radius is used in calculating the biaxial stress field ahead of the crack. The ratio of the transverse stress σ_2 to the longitudinal stress σ_1 acting on an element in the plastic zone (see fig. 2) is assumed equal to the stress ratio in front of a notch calculated by the theory of elasticity. These ratios are used in accounting for the influence of the state of stress on the stress-strain curve (see appendix A). In general, the stress ratio γ for any element in the plastic zone decreases as the applied load increases. This is partially supported by results from Swedlow's elastic-plastic analysis (ref. 1).

The internal-stress distribution in the plastic zone can now be written as a function of strain, strain rate, and the state of stress (see appendix A) as follows:

$$\bar{\sigma}(\xi) = \sigma_{y_o}\left(\frac{\dot{\bar{\epsilon}}}{\dot{\epsilon}_o}\right)^{m_o}\left(\frac{\bar{\epsilon}}{\epsilon_{y_o}}\right)^{n} F(\gamma,n) \tag{7}$$

where

$$n = n_o\left(\frac{\dot{\bar{\epsilon}}}{\dot{\bar{\epsilon}}_o}\right)^{p_o}$$

The strain and strain rate are given by equations (3) and (4), respectively.

In order to determine the constants A and B in equation (5), the condition that no stress singularity exists at the ends of the extended crack (assumption 3 in the Dugdale model) and the internal-stress distribution in the plastic zone (eq. (7)) are used to derive the plastic-zone size as a function of the material properties. This condition states that the elastic stress-intensity factor at the tip of the extended crack due to the external loading is equal to and of opposite sign to the stress-intensity factor due to the internal loading in the plastic zone. The stress-intensity factor for the external loading and that for the distributed stress on the crack boundary are obtained from reference 14. This condition may be expressed analytically as follows (refer to fig. 1):

$$\bar{k} = S\sqrt{c} = \frac{2\sqrt{c}}{\pi}\int_0^{\rho}\frac{\sigma(\xi)d\xi}{\sqrt{2c\xi - \xi^2}} \tag{8}$$

where

$$\sigma(\xi) = \frac{\bar{\sigma}(\xi)}{e^{\bar{\epsilon}}}$$

The stress distribution $\bar{\sigma}(\xi)$, equation (7), is divided by $e^{\bar{\epsilon}}$ to convert true stress to engineering stress in the plastic zone. The plastic-zone size is calculated by numerical integration of equation (8). (For the case when $\sigma(\xi)$ is constant and equal to the yield stress, eq. (8) is equivalent to Dugdale's solution for the plastic-zone size (eq. (1).)

PLASTIC-ZONE SIZE AND CRACK DISPLACEMENT CALCULATIONS

As a matter of interest, the influence of the strain-hardening exponent on the nondimensionalized plastic-zone size, ρ/a, is shown as a function of the applied stress level in figure 3. The material is assumed to be rate insensitive and the value of yield strain is taken to be 0.01. The values of strain-hardening exponent were varied from 0 to 0.5. The plastic-zone size was obtained by numerical integration of equation (8). The case for the strain-hardening exponent equal to zero corresponds to the elastic perfectly plastic case. However, it should be noted that this solution is not equivalent to that obtained by the original Dugdale model because the Dugdale model does not

account for the reduction in area and the state of stress at the tip of the crack. The broken curves represent the plastic-zone equation for the original Dugdale model and that from reference 5. The figure indicates that the amount of strain hardening has a large influence on the plastic-zone size and subsequently on the plasticity correction used in the modified Dugdale model analysis.

Similarly, the influence of stress rate on the plastic-zone size for AM-355 CRT is shown in figure 4 as a function of the applied stress level. The material constants which govern the stress-strain curve for this material were obtained experimentally from tensile test from the literature and are given in table I. Again the plastic-zone size is calculated from numerical integration of equation (8). The applied gross stress is normalized with respect to the yield stress at an elastic strain rate of approximately 0.005 per second. The gross stress rate was varied over several orders of magnitude. The decrease in plastic-zone size with an increase in stress rate is expected and has been observed by several investigators (ref. 15). This behavior indicates that for materials which are strain-rate sensitive, the gross stress rate applied to the plate influences the plastic-zone size and, consequently, the plasticity correction.

The modified Dugdale model equation for the crack boundary displacements for an infinite plate determined from the theory of elasticity is (refer to fig. 1(a))

$$2v(x,c) = \frac{4\sigma}{E}\sqrt{c^2 - x^2} - \frac{4}{\pi E}\int_0^{\rho} \sigma(\xi)\log\left|\frac{\sqrt{c^2 - x^2} - \sqrt{2c\xi - \xi^2}}{\sqrt{c^2 - x^2} + \sqrt{2c\xi - \xi^2}}\right| d\xi \qquad (9)$$

where

$$\sigma(\xi) = \frac{\bar{\sigma}(\xi)}{e^{\bar{\epsilon}}}$$

The crack displacement at any point of interest on the crack boundary is computed from equation (9) by substitution for the value of x.

The previous discussions on plastic-zone size and crack boundary displacements applied to an infinite plate. The finite width of a plate influences these parameters considerably and is accounted for as follows. The solution for an infinite periodic array of Dugdale model cracks (ref. 16) is used to account for the influence of finite width on the plastic-zone size for the modified model. The plastic-zone size is assumed to be of the form:

$$\rho = Aa\left[\frac{w}{\pi a}\ \text{arc sin}\left(\sin\frac{\pi a}{w}\sec\frac{\pi S}{2B\sigma_{y_o}}\right) - 1\right] \qquad (10)$$

This form is obtained by including the values of A and B from equation (5) into the plastic-zone expression for an infinite periodic array of Dugdale model cracks. This equation reduces to equation (5) when the crack length becomes small in comparison with the plate width.

FRACTURE CRITERION

In the present analysis, the external or internal stress-intensity factor, equation (8), provides a fracture toughness parameter $\bar{k}$. (This parameter is similar to Barenblatt's cohesive modulus (ref. 8).) As in the ASTM method, this modified stress-intensity factor is critical when the growth of the crack becomes unstable. The critical value $\bar{k}_c$ is obtained by use of the maximum gross stress, the critical crack length, and the plastic-zone size at failure. The fracture toughness equation for the modified Dugdale model is the left-hand portion of equation (8) and is given by the relation:

$$\bar{k}_c = S_{G_c}\sqrt{a_c + \rho}\ \alpha_p \tag{11}$$

The extended crack length c is written as $a_c + \rho$. The plastic zone is calculated by equation (10). The elastic-plastic width correction α_p is calculated by the following relation:

$$\alpha_p = 1 + 0.595\left(\frac{a_c + \rho}{b}\right)^2 + 0.481\left(\frac{a_c + \rho}{b}\right)^4 + 0.396\left(\frac{a_c + \rho}{b}\right)^6 + 0.337\left(\frac{a_c + \rho}{b}\right)^8 + 0.297\left(\frac{a_c + \rho}{b}\right)^{10} + 0.271\left(\frac{a_c + \rho}{b}\right)^{12} \tag{12}$$

The relation for α_p is the width-correction factor taken from reference 17 for the centrally cracked panel except that the actual crack length was replaced by the extended crack length.

In applying the model to the analysis of fracture data, an average value of fracture toughness calculated from equation (11) was used in predicting the maximum gross stress at failure on the panels. The application of equation (11) is limited to cases in which the plastic-zone size is less than the remaining net section. For the cases where the plastic zone does extend across the net section, the maximum gross stress at failure was calculated by the equation

$$S_{G_c} = \left(1 - \frac{2a_c}{w}\right)\left(\frac{\sigma_{y_o} + \sigma_{u_o}}{2}\right) \tag{13}$$

In order to apply equation (11) to practical applications, the critical crack length (crack length at maximum load) must be known before failure. From the studies of slow crack extension, the ratio of the critical crack length to the initial crack length is found to be a single-valued function of the crack-length to panel-width ratio regardless of width for a given material. This observation is upheld by a moderate amount of data obtained from the literature on plate specimens of various widths for several aluminum alloys, steels, and one titanium. The test data for the titanium alloy are unpublished NASA data. The following empirical equation is proposed to fit these data

$$\frac{a_c}{a_o} = 1 + C\left(\frac{w}{2a_o} - 1\right)^Z \tag{14}$$

where C and Z are assumed constant for a given material tested under identical loading and environmental conditions. This equation was fitted to the slow crack-growth data on the previously mentioned materials. The results are shown in figure 5. The constants C and Z are tabulated in table I.

METHODS OF FAILURE ANALYSIS

In the ASTM method, the fracture toughness value K_c is given by (ref. 5)

$$K_c = S_{G_c}\sqrt{w \tan\left(\frac{\pi a_c}{w} + \frac{K_c^2}{2w\sigma_y^2}\right)} \tag{15}$$

This equation is regarded valid only when the net section stress S_{N_c} is less than 0.8 of the yield stress.

In the Notch Strength Analysis method, the crack sensitivity is measured as C_m and is given by (ref. 7)

$$\frac{\sigma_u}{S_{N_o}} = 1 + C_m K_w \sqrt{a_o} \tag{16}$$

where

$$K_w = \sqrt{\frac{1 - \frac{2a_o}{w}}{1 + \frac{2a_o}{w}}}$$

is the width correction factor. This equation in the present form is regarded valid only when the initial net section stress S_{N_o} is less than the yield stress.

ANALYSIS OF TEST DATA

Tensile Properties and Test Conditions

In order to verify the proposed model, fracture data for several aluminum alloys and steels at room temperature were analyzed. The fracture data were obtained from the literature and are shown in tables II to VI. The tensile properties, material constants, and test conditions for the materials analyzed are shown in table I. The values of m_o, n_o, and p_o were determined from room temperature tensile tests conducted at strain rates ranging from 10^{-5} to 10^3 per second. The tensile data were obtained from the literature. The materials and references used to obtain the strain rate properties are noted in tables II to VI.

In most series of tests, the load rate was held constant and the specimen width was varied. The panel widths ranged from 3 to 48 inches. Thus, the gross stress rate applied to the panels varied considerably. However, the value of stress rate given in table I is an average value for the data analyzed.

In order to normalize the plastic-zone size with crack length, a constant ratio of crack velocity $\dot{a}$ to critical crack length a_c was assumed in equation (7). This ratio was estimated for each material analyzed and is given in table I. These estimates were based on crack velocity measurements made on aluminum alloys and on the equation (ref. 18):

$$\dot{a} = 0.38\sqrt{\frac{E}{D}}\left(1 - \frac{a_o}{a}\right) \tag{17}$$

This equation is derived for an elastic material and for a constant applied stress on an infinite plate. The crack velocities calculated by this equation are expected to be higher than the actual values due to the dissipation of energy in the plastic zone which is neglected in the development of equation (17).

Comparison of Methods

The objective of the following comparison of failure analysis methods is to demonstrate the overall usefulness of the methods in analyzing fracture data and to indicate any variation in the material constant for each method as a function of the test variables such as panel width and crack length.

The fracture toughness values computed by the modified Dugdale model for the materials analyzed are plotted as a function of width in figure 6. The toughness values computed by the ASTM method and the crack sensitivity values for the NSA methods are also shown for some of the materials analyzed.

The toughness values calculated by the proposed model and the ASTM method for 2219-T87 aluminum-alloy sheet are shown in figures 6(a) and 6(b),

respectively. The values computed by the ASTM method show a consistent variation with width and also with crack length at a panel width of 24 inches. The values calculated by the proposed model were nearly constant. Likewise, the crack sensitivity values calculated by the NSA method (not shown in this fig.) were very nearly constant. The solid symbols indicate data which did exceed the limitations for the ASTM method. In contrast to the ductile behavior of 2219-T87, the values computed by the proposed model and the NSA method for 7075-T6 aluminum-alloy sheet, are shown in figures 6(c) and 6(d), respectively. The values calculated by the NSA approach varied systematically with width. However, in this case the toughness values computed by the proposed model and the ASTM method (not shown in the fig.) were nearly constant. The primary difference between the correlation of fracture data for the two previously mentioned materials results from the fact that 7075-T6 is brittle in comparison with 2219-T87. The calculated plastic-zone size at failure by the proposed model for the 7075-T6 was only one-sixth that calculated for 2219-T87. The fracture toughness values computed by the modified Dugdale model for the other materials analyzed are shown in figures 6(e) to 6(g). The values calculated are very nearly constant.

In order to compare the usefulness of the methods in calculating the maximum gross stress at failure, the predicted results for two aluminum alloys are shown in figure 7. This figure shows the ratio of experimental to calculated gross stress at failure as a function of panel width. The predicted results for the 2219-T87 aluminum-alloy sheet are shown for the proposed model and the ASTM method in figures 7(a) and 7(b), respectively. The fracture toughness values used in the predictions were determined from an average value calculated from test data which did not exceed the limitations for each method. These values are shown in figures 6(a) and 6(b), respectively. The ratio of experimental to calculated stress for the ASTM method shows a variation as the panel width decreases. This is evident from the variation in toughness as shown in figure 6(b). The proposed model and the NSA method (not shown in the fig.) gave very consistent predictions for this material. The gross stress predictions for the NSA method are shown in table II. The solid symbols indicate data which did exceed the limitation for each method. Likewise, the predicted results for the proposed model and the NSA method for 7075-T6 aluminum-alloy sheet are shown in figures 7(c) and 7(d), respectively. In this case, the ASTM method gave essentially the same results as the proposed model. However, the NSA method gave a consistent variation in the ratio of experimental to calculated gross stress as the panel width decreased. This is again evident in the variation of the crack sensitivity values with width in figure 6(d). In general, these trends persisted for the other materials.

Tables II through VI present the tabulated results of predictions computed by the ASTM method, the NSA method, and the modified Dugdale model on the basis of predicting maximum gross stress at failure. The fracture toughness value computed by each method is determined from an average value calculated from test data which did not exceed the limitations for each method. These values are noted in the tables. The average percentage error in predicting maximum gross stress at failure is shown for each method in the tables. The percentage error in parenthesis for the modified Dugdale model is obtained from predicting the gross stress at failure by using the slow crack extension equation with the

model, instead of the actual values of critical crack length. As a note of interest, the plastic-zone size at failure as calculated by the proposed model, was nearly constant for a given material.

Finally, a table of predicted results indicates the accuracy of each method in predicting the maximum gross stress at failure for all of the fracture data analyzed. The table shows the percentage error in predicting stress and the number of data points which fall in the appropriate range. The total number of test data analyzed was 92. It may be seen that the accuracy of the proposed model is somewhat better than NSA method and substantially better than the ASTM method. The number in parenthesis is the number of data points which exceeded the limitations for each method.

TABLE OF PREDICTED RESULTS

Method	No. of data points with gross stress error of -				
	0% to 5%	5% to 10%	10% to 15%	15% to 20%	>20%
MDM	79 (8)*	10 (2)	2	1	0
NSA	63 (5)	20 (1)	3	4	2
ASTM	37 (9)	31 (14)	17 (15)	4 (3)	3 (2)

*The number in parenthesis indicates the number of data points which exceeded the limitation for each corresponding method.

CONCLUSIONS

The Dugdale model has been extended to include the influence of the stress-strain curve on the plastic-zone size. Fracture data for several materials were analyzed according to the modified Dugdale model and by the ASTM and NSA methods. The analysis and observations made on the fracture process support the following conclusions for the materials analyzed:

1. The modified Dugdale model gave gross stress predictions that were more consistent with the test data than the ASTM and NSA methods.

2. The modified Dugdale model gave fracture toughness values which were nearly constant regardless of width. In contrast, the values calculated by the ASTM and NSA methods varied as a function of width for some of the materials analyzed.

3. The calculated plastic-zone size at failure was nearly constant for a given material.

4. The ratio of critical-to-initial crack length was a single-valued function of the crack length-to-panel width ratio regardless of width for a given material.

APPENDIX A

STRESS-STRAIN CURVE

The shape of the stress-strain curve is influenced by factors such as strain-hardening, strain rate, the state of stress and temperature. In this case, the true stress-true strain curve is considered more useful than the engineering stress-strain curve, particularly in the plastic range, because the curve can be described by a single-valued function.

For a large quantity of test data on tensile stress-strain curves, at constant temperature and constant strain rate the stress increases with strain according to the relation (ref. 23).

$$\bar{\sigma} = C_1 \bar{\epsilon}^n \Big|_{\dot{\bar{\epsilon}},T} \tag{A1}$$

where C_1 is a constant and n is the strain-hardening exponent. The constant C_1 is equal to the yield stress when the strain is normalized with respect to the yield strain. The stress-strain curves can be expressed by the form

$$\bar{\sigma} = \sigma_y \left(\frac{\bar{\epsilon}}{\epsilon_y}\right)^n \Big|_{\dot{\bar{\epsilon}},T} \tag{A2}$$

if the true yield stress and engineering yield stress are assumed to be equal. This equation is considered to be applicable for stresses in the plastic range. The influence of strain rate has also been shown to agree with a power law within certain ranges. The stress at a given strain and temperature increases with the strain rate by the relation (ref. 23)

$$\bar{\sigma} = D_1 \left(\dot{\bar{\epsilon}}\right)^m \Big|_{\bar{\epsilon},T} \tag{A3}$$

where D_1 is a constant and m is the strain-rate exponent. The influence of both strain and strain rate can be expressed in a single equation by the expression

$$\bar{\sigma} = \sigma_{y_o} \left(\frac{\dot{\bar{\epsilon}}}{\dot{\epsilon}_o}\right)^{m_o} \left(\frac{\bar{\epsilon}}{\epsilon_{y_o}}\right)^n \Big|_T \tag{A4}$$

which applies for a given temperature T. In order to approximate the shape of the stress-strain curve, the values of yield stress σ_{y_o} and yield strain ϵ_{y_o} are obtained from tensile tests at an elastic strain rate, $\dot{\bar{\epsilon}}_o$, of 0.005 per second. The exponent m_o is evaluated from tensile tests from the variation in the yield stress with strain rate. The strain-hardening exponent n also varies as a function of strain rate and is evaluated by the expression

$$n = n_o\left(\frac{\dot{\bar{\epsilon}}}{\dot{\bar{\epsilon}}_o}\right)^{p_o} \tag{A5}$$

where n_o is the value calculated from the strain-rate test at $\dot{\bar{\epsilon}}_o$.

The influence of the biaxial state of stress ahead of the crack on the stress-strain curve is computed from the deformation theory of plastic flow. From the assumption that the material maintains constant volume under plastic deformation, the stress-strain curve has the following relation (ref. 23):

$$\bar{\sigma} = C_1\bar{\epsilon}^n F(\gamma,n) \tag{A6}$$

where

$$F(\gamma,n) = \frac{2^n}{\left(\gamma^2 - \gamma + 1\right)^{\frac{1-n}{2}}(2 - \gamma)^n}$$

and

$$\gamma = \frac{\sigma_2}{\sigma_1}$$

the ratio of transverse to longitudinal stress, see figure 2.

The final equation for the stress-strain curve is given as follows:

$$\bar{\sigma} = \sigma_{y_o}\left(\frac{\dot{\bar{\epsilon}}}{\dot{\bar{\epsilon}}_o}\right)^{m_o}\left(\frac{\bar{\epsilon}}{\epsilon_{y_o}}\right)^n F(\gamma,n)\Big|_T \tag{A7}$$

where

$$n = n_o\left(\frac{\dot{\bar{\epsilon}}}{\dot{\bar{\epsilon}}_o}\right)^{p_o}$$

APPENDIX B

METHOD FOR CALCULATING THE CONSTANTS A AND B

The method used to evaluate the constants A and B employs successive approximation of the plastic-zone size (eq. (5)) until the plastic-zone size calculated from equation (5) is equal to that calculated by numerical integration of equation (8). In other words, the final plastic-zone size is used in calculating the influence of strain, strain rate, and the state of stress. The steps are listed as follows:

1. An initial estimate for the values of A_i and B_i is made.

2. The plastic-zone size, equation (5), is calculated by using A_i and B_i.

3. The crack tip displacement or notch root radius is calculated from the approximate expression

$$v_a = r = \frac{4aB_i\sigma_y}{\pi E} \ln\left(\frac{\rho}{A_i a} + 1\right) \tag{B1}$$

which gives the displacement or root radius in terms of the plastic-zone size and the values A_i and B_i. This expression is obtained from equations (1) and (2) by replacing σ_y with $B_i\sigma_y$ and ρ with ρ/A_i.

4. The internal-stress distribution $\sigma(\xi)$ (eq. (7)), is calculated as a function of strain, strain rate, and the state of stress by using equations (3) and (4) and the results of steps 2 and 3. In equation (8), the plastic-zone size ρ is chosen and the stress S is calculated by numerical integration. A wide range of ρ values is chosen.

5. Equation (5) is fitted to the plastic-zone size calculated by step 4. This curve gives a new set of values of A_{i+1} and B_{i+1}. The value of B_{i+1} is determined by the asymptote for the calculated plastic-zone size, step 4. The asymptote cannot be determined exactly; however, the calculated curve does approach the asymptote very rapidly. A sufficiently large value of ρ is chosen to obtain the value of B_{i+1}. The value of A_{i+1} is determined by using equation (5) together with B_{i+1}. The value of A_{i+1} is chosen to fit the calculated curve.

6. This procedure is repeated until the values of both A and B converge individually.

REFERENCES

1. Swedlow, J. L.: The Thickness Effect and Plastic Flow in Cracked Plates. Aerospace Research Laboratories, ARL65-216, Wright-Patterson Air Force Base, Oct. 1965.

2. Ault, R. T.; and Spretnak, J. W.: Initial Yielding and Fracture in Notched Sheet Molybdenum. Int. Jour. Mech. Sciences, vol. 7, 1965, pp. 87-102.

3. Stimpson, L. D.; and Eaton, D. M.: The Extent of Elasto-Plastic Yielding at the Crack Point of an Externally-Notched Plane-Stress Tensile Specimen. ARL 24, Aerospace Research Laboratories, Wright-Patterson Air Force Base, July 1961.

4. Dugdale, D. S.: Yielding of Steel Sheets Containing Slits. Jour. Mech. Phys. Solids, vol. 8, 1960.

5. ASTM Special Committee on Fracture Testing of High-Strength Metallic Materials: Fracture Testing of High-Strength Sheet Materials, ASTM Bull. 243, Jan. 1960.

6. Kuhn, P.; and Figge, I. E.: Unified Notch-Strength Analysis for Wrought Aluminum Alloys. NASA TN D-1259, 1962.

7. Kuhn, P.: Residual Strength in the Presence of Fatigue Cracks (Part I). Presented to the Structures and Materials Panel - AGARD, Turin, Italy, April 17, 1967.

8. Barenblatt, G. I.: Mathematical Theory of Equilibrium Cracks in Brittle Fracture. Advances in Applied Mechanics, vol. VII, Academic Press, 1962.

9. Goodier, J. N.; and Field, F. A.: Plastic Energy Dissipation in Crack Propagation. Fracture of Solids (eds. Drucker and Gilman), Wiley, 1963.

10. Rosenfield, A. R.; Dai, P. K.; and Hahn, G. T.: Crack Extension and Propagation Under Plane Stress. Presented at the International Conference on Fracture, Sendai, Japan, Sept. 1965.

11. Forman, R. G.: Experimental Program to Determine Effect of Crack Buckling and Specimen Dimensions on Fracture Toughness of Thin Sheet Materials. AFFDL-TR-65-146, Wright-Patterson Air Force Base, Jan. 1966.

12. Gerberich, W. W.: Plastic Strains and Energy Density in Cracked Plates, Part I - Experimental Technique and Results, Experimental Mech., pp. 335-344, Nov. 1964.

13. Rice, J. R.: Stresses Due to a Sharp Notch in a Work Hardening Elastic Plastic Material Loaded by Longitudinal Shear. Brown Univ. Tech. Report, NSF GK-286/1, Dec. 1965.

14. Paris, P.; and Sih, G.: Stress Analysis of Cracks. Fracture Toughness Testing, ASTM STP 381, 1964.

15. Forman, R. G.: High Strain Rate Tear Tests. Test Progress Report 51-R-1. The Boeing Airplane Co., Seattle, Washington, July 1961.

16. Rice, J. R.: The Mechanics of Crack Tip Deformation and Extension by Fatigue. Brown Univ. Tech. Rept., NSF GK-286/3, May 1966.

17. Isida, M.: Crack Tip Stress Intensity Factors for the Tension of an Eccentrically Cracked Strip. Dept. of Mech., Lehigh Univ., 1965.

18. Dulaney, E. N.; and Brace, W. F.: Velocity Behavior of a Growing Crack. Jour. Appl. Phys., vol. 31, 1960, p. 2233.

19. Eichenberger, T. W.: Fracture Resistance Data Summary Report DA-20947. The Boeing Airplane Company, Seattle, Washington, June 1962.

20. Kattus, J. R.: Tensile Properties of Aircraft-Structural Metals at Various Rates of Loading After Rapid Heating. WADC TR 58-440, May 1959.

21. Maider, C. J.; and Green, S. J.: Compressive Strain Rate Tests on Six Selected Materials at Strain Rates From 10^{-3} to 10^{4} Inch/Inch/Second. GM Defense Research Lab., May 1965.

22. Kendall, D. P.: The Effect of Strain Rate of Yielding in High-Strength Steels, WVT 6618, May 1966.

23. Spretnak, J. W.: A Summary of the Theory of Fracture in Metals. Defense Metals Information Center, Report 157, 1961.

TABLE I.- TENSILE PROPERTIES, MATERIAL CONSTANTS,

AND TEST CONDITIONS

Material	2219-T87	7075-T6	AM 355 CRT	4330	4330
Nominal thickness, in.	0.10	0.065	0.02	0.08	0.14
(a) σ_{u_o}, ksi	69.4	84.8	240.8	223.0	222.4
(a) σ_{y_o}, ksi	58.5	75.5	222.4	199.4	189.9
(a) n_o	0.092	0.082	0.068	0.077	0.093
m_o	0.004	0.005	0.032	0.007	0.007
p_o	-0.022	-0.023	-0.015	-0.010	-0.010
A	0.698	0.693	0.702	0.696	0.695
B	1.026	1.025	1.140	1.048	1.056
C	0.115	0.020	0.162	0.173	0.250
Z	0.643	1.518	0.569	0.568	0.529
$\dot{S}$, ksi/sec	70	100	200	80	50
$\dot{a}/a_c$, 1/sec	100	200	100	800	800

(a) $\dot{\bar{\epsilon}}_o \approx 0.005$ in./in./sec at room temperature.

TABLE II.- EXPERIMENTAL AND PREDICTED RESULTS FOR 2219-T87, LONGITUDINAL GRAIN (REF. 19) (a)

w, in.	$2a_o$, in.	$2a_c$, in.	S_{exp}, ksi	S_{N_c}/σ_{y_o}	S_{exp}/S_{calc}			$\bar{k}_c$, $lbf\text{-}in^{-3/2}$	ρ, in.
					ASTM (b)	NSA (c)	MDM (d)		
3.5	0.75	0.98	46.4	1.10	0.93	1.10	1.01	(e)	(e)
6.0	2.0	2.46	34.6	1.00	0.89	1.05	1.01	68,600	0.85
12.0	2.0	2.68	41.3	0.91	0.94	1.06	1.01	73,700	1.17
12.0	4.0	4.77	27.9	0.79	0.85	0.95	0.90	59,700	1.04
18.0	4.0	5.26	34.0	0.82	1.01	1.04	1.03	76,000	1.17
24.0	0.5	0.77	54.4	0.96	0.85	1.03	1.01	77,400	1.38
24.0	1.0	1.40	48.4	0.89	0.87	1.02	0.98	66,900	1.35
24.0	2.0	2.59	42.4	0.81	0.92	1.02	0.97	68,100	1.31
24.0	4.0	5.73	33.9	0.76	1.02	0.99	1.02	74,600	1.22
24.0	8.0	9.58	24.1	0.68	0.96	0.95	0.96	68,200	1.12
24.0	12.0	13.65	17.8	0.71	0.93	0.94	0.95	68,600	1.00
24.0	18.0	18.62	8.40	0.64	(f)	----	----	------	----
24.0	18.0	19.43	9.45	0.85	----	----	----	------	----
24.0	20.0	20.65	6.44	0.79	----	----	----	------	----
36.0	4.0	5.45	34.0	0.68	0.99	0.96	0.97	69,000	1.28
48.0	4.0	5.58	34.9	0.67	1.01	0.96	0.99	71,600	1.30
48.0	8.0	9.25	28.2	0.60	1.03	0.97	0.98	70,600	1.26
48.0	12.0	15.05	23.2	0.59	1.09	0.94	1.03	75,300	1.20
48.0	12.0	14.2	24.5	0.60	1.11	0.99	1.05	77,400	1.21
48.0	24.0	25.72	15.4	0.57	1.04	0.96	1.01	74,200	1.07
48.0	36.0	37.17	7.90	0.60	----	----	----	------	----
48.0	41.9	43.18	4.34	0.74	----	----	----	------	----
Average percentage error in gross stress					6.9%	4.2%	2.8% (3.1%)		

(a) Strain-rate data for 2014-T6 (ref. 20).

(b) K_c = 113,000 $lbf\text{-}in^{-3/2}$.

(c) C_m = 0.58 $in^{-1/2}$.

(d) $\bar{k}_c$ = 72,300 $lbf\text{-}in^{-3/2}$.

(e) Plastic zone extends the net section.

(f) Data was not analyzed because $\frac{2a_o}{w} > 0.75$.

TABLE III.- EXPERIMENTAL AND PREDICTED RESULTS FOR 7075-T6, TRANSVERSE GRAIN (REF. 11) (a)

w, in.	$2a_o$, in.	$2a_c$, in.	S_{exp}, ksi	S_{N_c}/σ_{y_o}	S_{exp}/S_{calc}			$\bar{k}_c$, $lbf\text{-}in^{-3/2}$	ρ, in.
					ASTM (b)	NSA (c)	MDM (d)		
3.03	0.75	0.83	44.5	0.81	0.95	1.17	1.01	39,000	0.20
4.50	1.126	1.126	38.2	0.67	0.90	1.09	0.94	35,000	0.20
4.50	1.126	1.226	38.2	0.69	0.94	1.09	0.98	37,200	0.20
6.00	1.50	1.70	33.0	0.61	0.94	1.01	0.96	36,200	0.20
7.00	3.00	3.12	23.4	0.56	0.93	1.01	0.96	36,600	0.19
8.00	3.00	3.44	23.9	0.55	0.99	0.98	1.01	38,900	0.19
10.0	2.25	2.50	30.0	0.53	1.00	1.00	1.00	38,200	0.20
10.0	3.00	3.26	28.1	0.55	1.08	1.08	1.08	42,200	0.20
12.0	3.00	3.50	25.2	0.47	0.99	0.93	0.98	37,500	0.20
12.0	3.00	3.00	26.6	0.47	0.96	0.98	0.96	36,000	0.20
15.0	3.75	4.00	24.3	0.44	1.00	0.96	1.00	38,100	0.20
16.0	3.00	3.40	28.0	0.47	1.06	0.99	1.05	40,400	0.21
18.0	4.50	5.50	21.1	0.40	1.03	0.88	1.01	38,800	0.20
20.0	3.00	3.60	27.1	0.44	1.05	0.91	1.03	39,500	0.21
21.0	5.25	6.25	20.3	0.38	1.05	0.88	1.02	39,600	0.20
22.0	3.00	3.52	27.3	0.43	1.04	0.94	1.02	39,200	0.21
24.0	3.00	7.00	17.6	0.33	0.96	0.80	0.94	35,700	0.20
24.0	3.00	7.10	20.1	0.38	1.10	0.92	1.08	41,500	0.20
Average percentage error in gross stress					4.7%	7.0%	3.2% (4.2%)		

(a) Strain-rate data for 7075-T6 (ref. 21).

(b) K_c = 64,200 $lbf\text{-}in^{-3/2}$.

(c) C_m = 1.43 $in^{-1/2}$.

(d) $\bar{k}_c$ = 38,300 $lbf\text{-}in^{-3/2}$.

TABLE IV.- EXPERIMENTAL AND PREDICTED RESULTS FOR AM-355 CRT, LONGITUDINAL GRAIN (REF. 11) (a)

w, in.	$2a_o$, in.	$2a_c$, in.	S_{exp}, ksi	S_{N_c}/σ_{y_o}	S_{exp}/S_{calc}			$\bar{k}_c$, lbf-in$^{-3/2}$	ρ, in.
					ASTM (b)	NSA (c)	MDM (d)		
6.00	2.00	2.40	123.3	0.92	0.90	1.08	0.95	194,500	0.53
7.00	4.00	4.70	75.0	1.02	0.95	1.04	1.01	223,800	0.43
8.00	4.00	4.80	84.0	0.94	0.94	1.03	1.00	216,800	0.47
9.00	3.00	3.60	108.6	0.81	0.91	1.01	0.92	193,300	0.56
12.0	4.00	4.90	100.3	0.76	0.94	0.98	0.95	203,100	0.57
12.0	4.00	4.94	107.0	0.82	1.01	1.05	1.02	224,800	0.57
15.0	5.00	6.50	93.0	0.74	1.00	0.95	1.00	217,100	0.57
16.0	4.00	5.30	109.0	0.73	1.02	0.99	1.00	219,400	0.60
18.0	6.00	7.50	88.5	0.68	1.00	0.94	0.99	214,700	0.58
20.0	4.00	5.20	120.0	0.73	1.08	1.04	1.06	234,600	0.62
21.0	7.00	8.40	86.0	0.64	1.01	0.94	0.99	215,800	0.59
24.0	4.00	5.74	122.0	0.72	1.14	1.02	1.10	248,800	0.63
24.0	8.00	9.60	84.0	0.63	1.05	0.95	1.02	224,200	0.59
Average percentage error in gross stress					5.2%	4.4%	3.4% (4.0%)		

(a) Strain-rate data for AM-350 (ref. 20).

(b) K_c = 354,000 lbf-in$^{-3/2}$.

(c) C_m = 0.57 in$^{-1/2}$.

(d) $\bar{k}_c$ = 218,000 lbf-in$^{-3/2}$.

TABLE V.- EXPERIMENTAL AND PREDICTED RESULTS FOR 4330,

t = 0.08 INCH, LONGITUDINAL GRAIN (REF. 19) (a)

w, in.	$2a_o$, in.	$2a_c$, in.	S_{exp}, ksi	S_{N_c}/σ_{y_o}	S_{exp}/S_{calc}			$\bar{k}_c$, $lbf\text{-}in^{-3/2}$	ρ, in.
					ASTM (b)	NSA (c)	MDM (d)		
3.0	1.02	1.25	114.3	0.98	0.85	0.95	0.93	(e)	(e)
3.0	1.03	1.25	118.4	1.02	0.88	0.99	0.96	(e)	(e)
5.0	0.85	1.10	160.2	1.03	0.91	1.08	1.01	225,800	0.70
5.0	0.41	0.80	169.8	1.01	0.87	0.98	1.02	207,400	0.73
5.0	0.12	0.30	195.6	1.04	0.82	0.97	1.02	228,700	0.79
5.0	1.4	1.87	126.1	1.01	0.92	1.02	1.03	210,300	0.62
5.0	0.81	1.13	152.6	0.99	0.88	1.02	1.00	195,900	0.70
5.0	0.38	0.75	178.9	1.05	0.90	1.01	1.00	(e)	(e)
5.0	0.14	0.30	194.8	1.04	0.82	0.98	1.01	218,600	0.79
5.0	1.42	1.82	117.8	0.93	0.85	0.95	0.95	172,000	0.63
5.0	0.39	0.82	183.9	1.10	0.95	1.05	1.04	(e)	(e)
5.0	1.4	1.87	126.9	1.02	0.93	1.02	1.04	214,000	0.62
5.0	1.0	1.43	135.5	0.95	0.86	0.96	0.97	180,000	0.67
5.0	1.0	1.35	138.6	0.95	0.86	0.98	0.97	179,200	0.68
5.0	1.0	1.53	142.3	1.03	0.93	1.01	1.05	224,000	0.66
5.0	1.0	1.57	140.8	1.03	0.93	1.00	1.05	224,500	0.65
5.0	1.0	1.61	145.7	1.08	0.98	1.03	1.02	(e)	(e)
5.0	1.0	1.55	148.2	1.08	0.99	1.05	1.02	(e)	(e)
5.0	0.38	0.60	178.9	1.02	0.85	1.01	1.01	206,400	0.76
5.0	1.42	1.73	128.2	0.98	0.90	1.04	1.00	196,200	0.63
5.0	1.60	2.05	118.5	1.01	0.92	1.02	1.02	207,000	0.60
5.0	0.10	0.18	198.8	1.03	0.79	0.97	1.00	191,600	0.80
5.0	0.37	0.65	166.4	0.96	0.81	0.94	0.96	163,500	0.75
5.0	0.10	0.20	199.5	1.04	0.80	0.98	1.01	216,300	0.80
5.0	0.77	0.95	156.4	0.97	0.85	1.02	0.98	180,200	0.72
6.0	2.0	2.33	118.8	0.97	0.93	1.06	1.02	209,400	0.64
12.0	1.99	2.80	134.0	0.88	1.02	1.02	1.06	226,500	0.79
12.0	2.52	3.24	97.9	0.67	0.79	0.80	0.82	151,400	0.77
18.0	4.00	5.26	111.7	0.79	1.10	1.00	1.11	239,000	0.78
24.0	1.98	3.00	132.5	0.76	1.00	0.94	1.01	210,000	0.84
36.1	1.98	3.21	137.2	0.75	1.06	0.95	1.07	227,100	0.85
48.1	2.01	3.48	133.0	0.72	1.06	0.92	1.06	223,100	0.86
Average percentage error in gross stress					11%	3.8%	3.6% (3.8%)		

(a) Strain-rate data for 4330 (ref. 22).

(b) K_c = 330,000 $lbf\text{-}in^{-3/2}$.

(c) C_m = 0.546 $in^{-1/2}$.

(d) $\bar{k}_c$ = 205,000 $lbf\text{-}in^{-3/2}$.

(e) Plastic zone extends the net section.

TABLE VI.- EXPERIMENTAL AND PREDICTED RESULTS FOR 4330,

t = 0.14 INCH, LONGITUDINAL GRAIN (REF. 19) (a)

w, in.	$2a_o$, in.	$2a_c$, in.	S_{exp}, ksi	S_{N_c}/σ_{y_o}	S_{exp}/S_{calc}			$\bar{k}_c$, $lbf\text{-}in^{-3/2}$	ρ, in.
					ASTM (b)	NSA (c)	MDM (d)		
1.56	0.51	0.51	115.6	0.90	1.66	1.02	1.02	(e)	(e)
3.00	1.01	1.45	99.0	1.01	0.88	0.97	0.93	(e)	(e)
3.00	1.51	1.97	68.5	1.05	1.08	0.90	0.97	(e)	(e)
6.00	2.00	2.68	91.0	0.87	0.85	1.00	0.93	155,500	0.54
12.0	2.00	3.16	120.7	0.86	1.07	1.14	1.10	212,000	0.67
24.0	2.00	3.75	101.4	0.63	0.93	0.90	0.93	162,900	0.71
36.0	0.5	1.65	158.3	0.87	1.05	1.04	1.11	226,800	0.75
36.0	1.0	4.57	106.8	0.64	1.06	0.80	1.04	191,000	0.71
36.0	1.96	6.96	79.5	0.52	0.96	0.69	0.94	165,500	0.70
36.0	4.0	6.00	93.1	0.59	1.05	1.00	1.02	184,900	0.70
36.0	8.0	10.0	69.6	0.51	1.01	0.97	0.98	176,100	0.67
48.0	2.0	11.85	64.0	0.45	1.00	0.55	0.95	171,600	0.68
Average percentage error in gross stress					11.3%	11.8%	5.5% (11.6%)		

(a) Strain-rate data for 4330 (ref. 22).

(b) K_c = 294,000 $lbf\text{-}in^{-3/2}$.

(c) C_m = 0.89 $in^{-1/2}$.

(d) $\bar{k}_c$ = 183,000 $lbf\text{-}in^{-3/2}$.

(e) Plastic zone extends the net section.

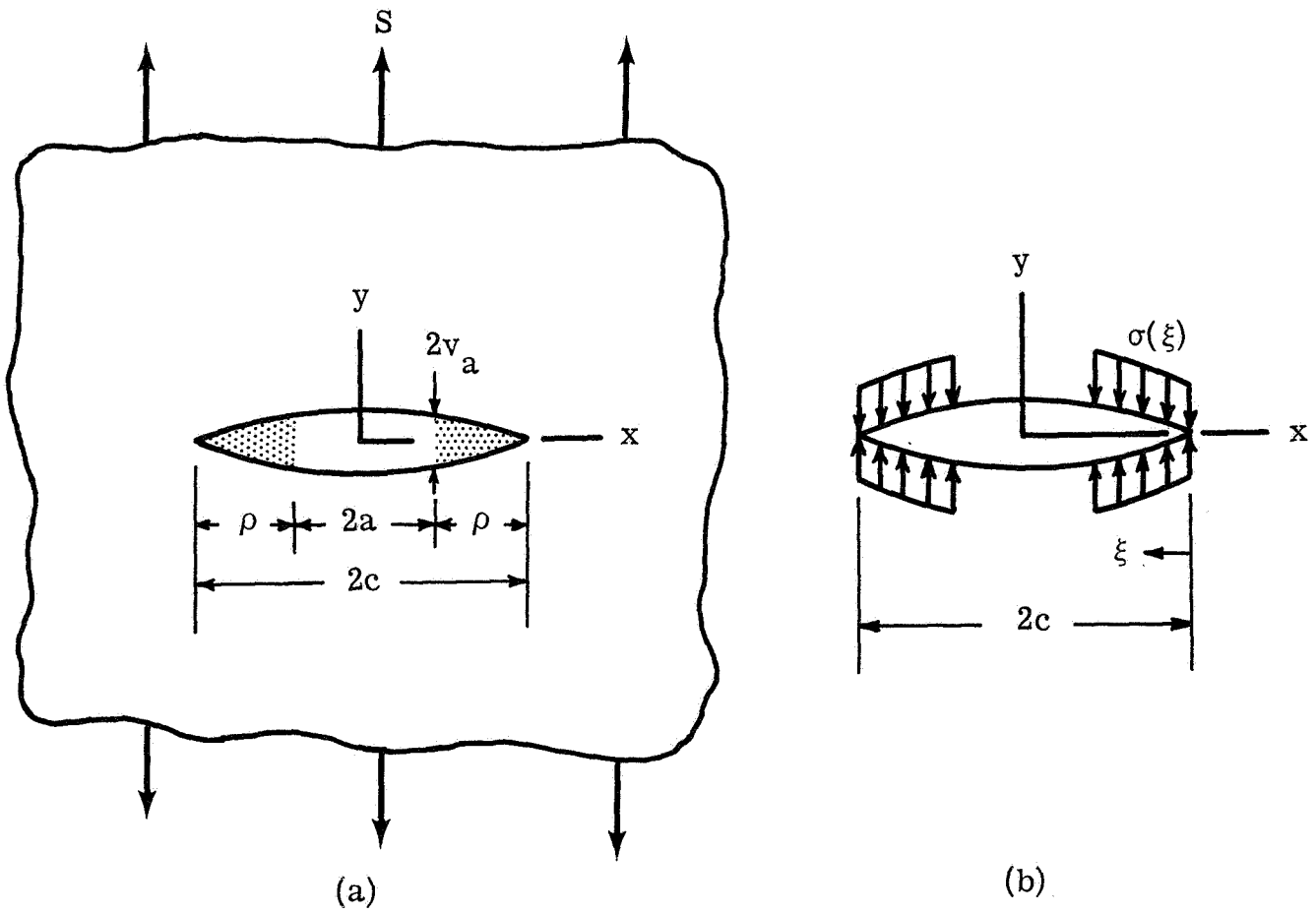

Figure 1.- Dugdale's model for plastic yielding at the tip of a crack.

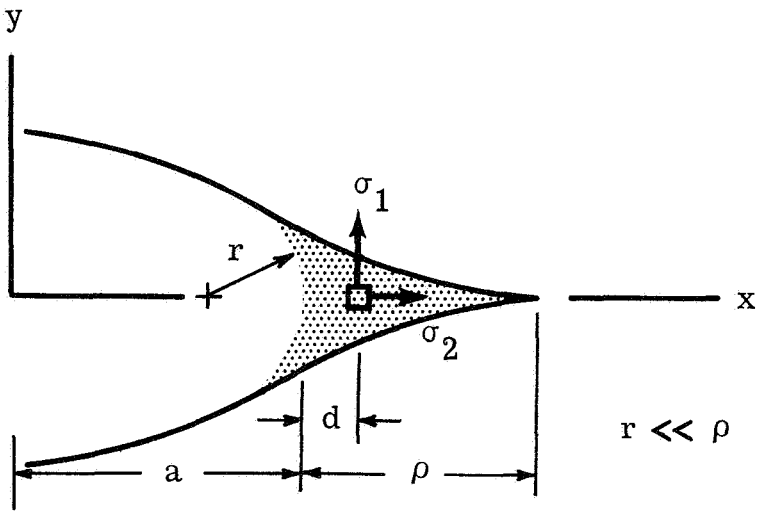

Figure 2.- Model of crack tip with root radius and plastically deformed material.

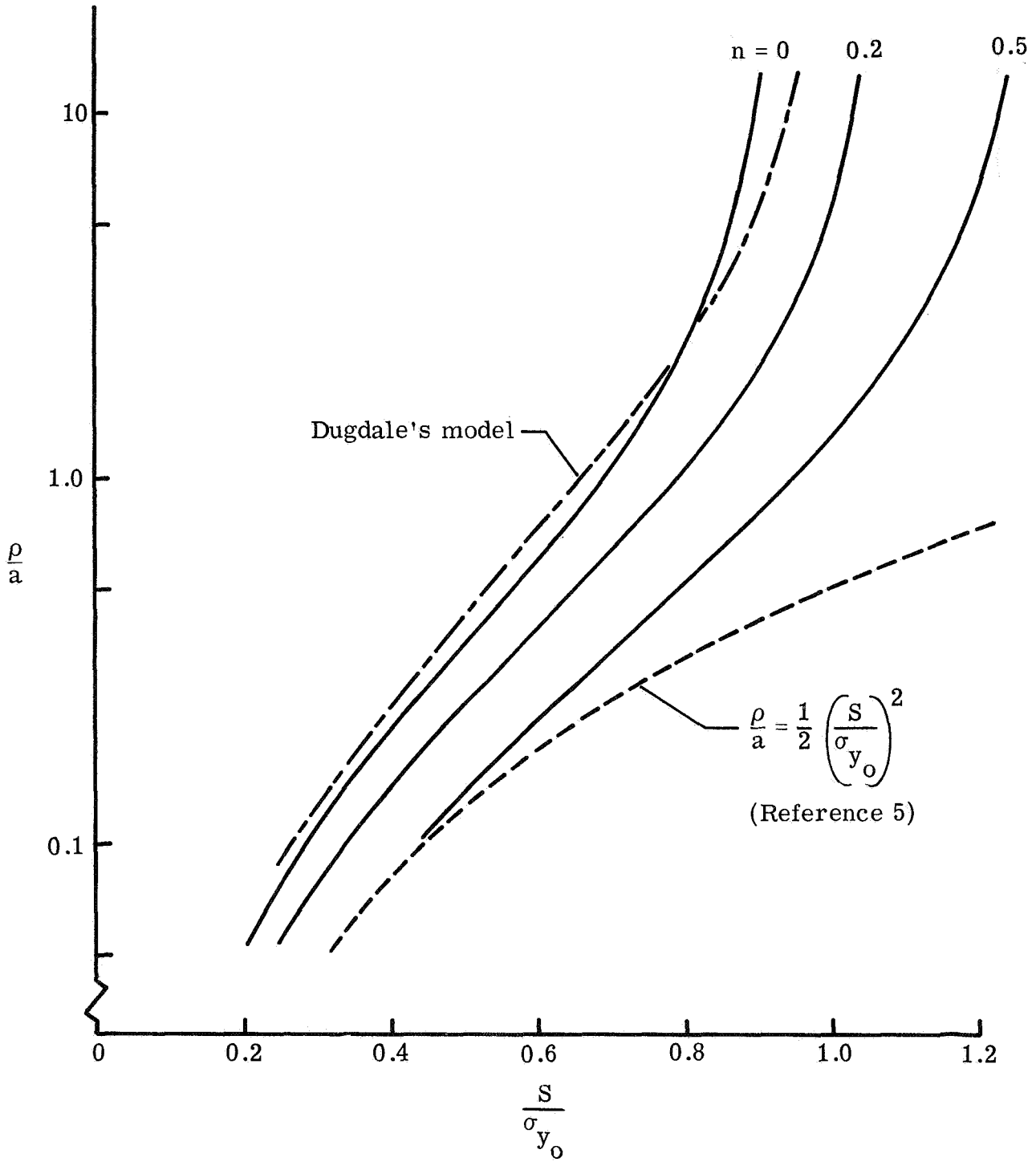

Figure 3.- Strain-hardening effects on the plastic-zone size for a rate-insensitive material ($\epsilon_y = 0.01$).

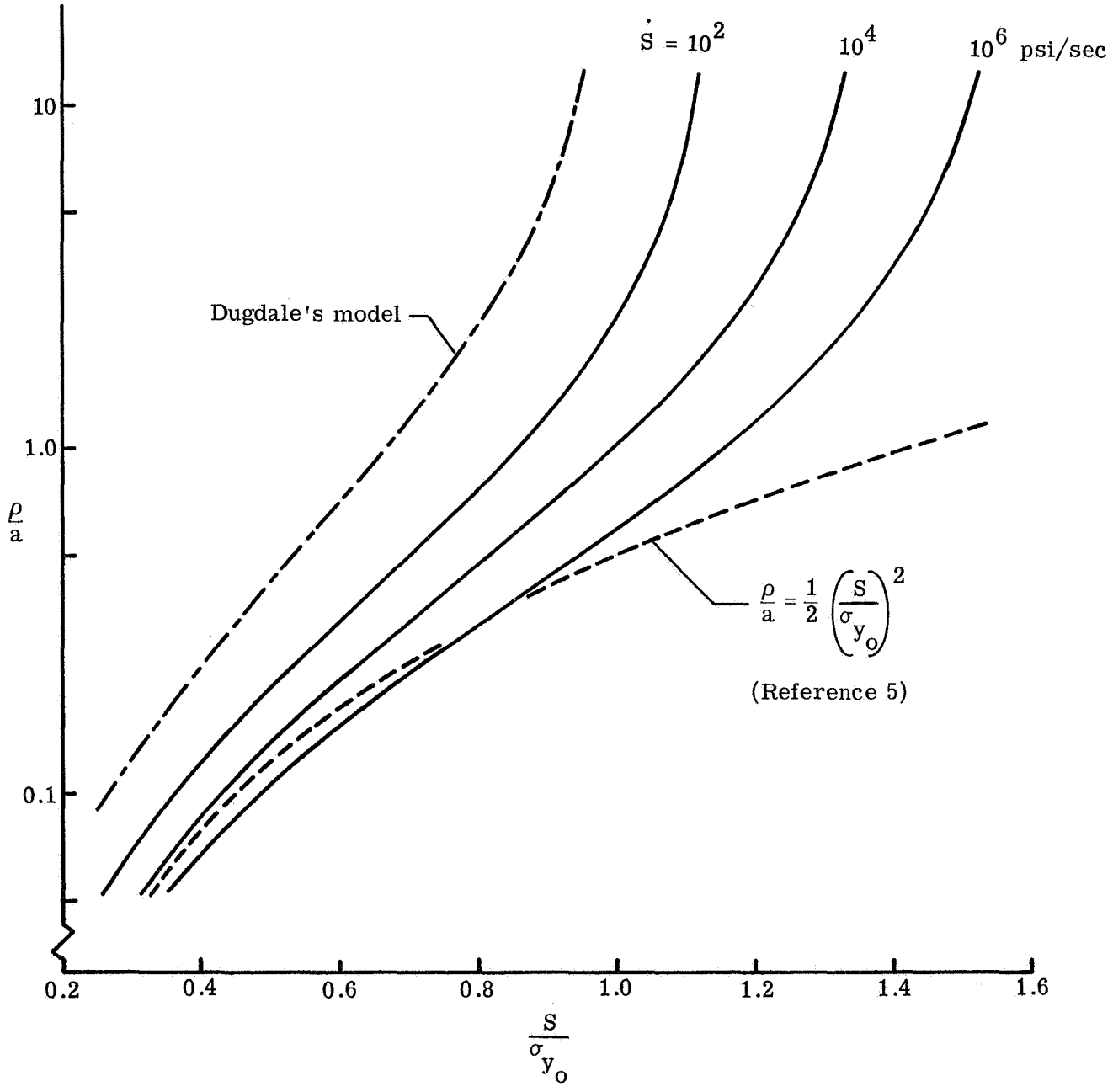

Figure 4.- Stress-rate effects on the plastic zone size for a rate-sensitive material, AM-355 CRT.

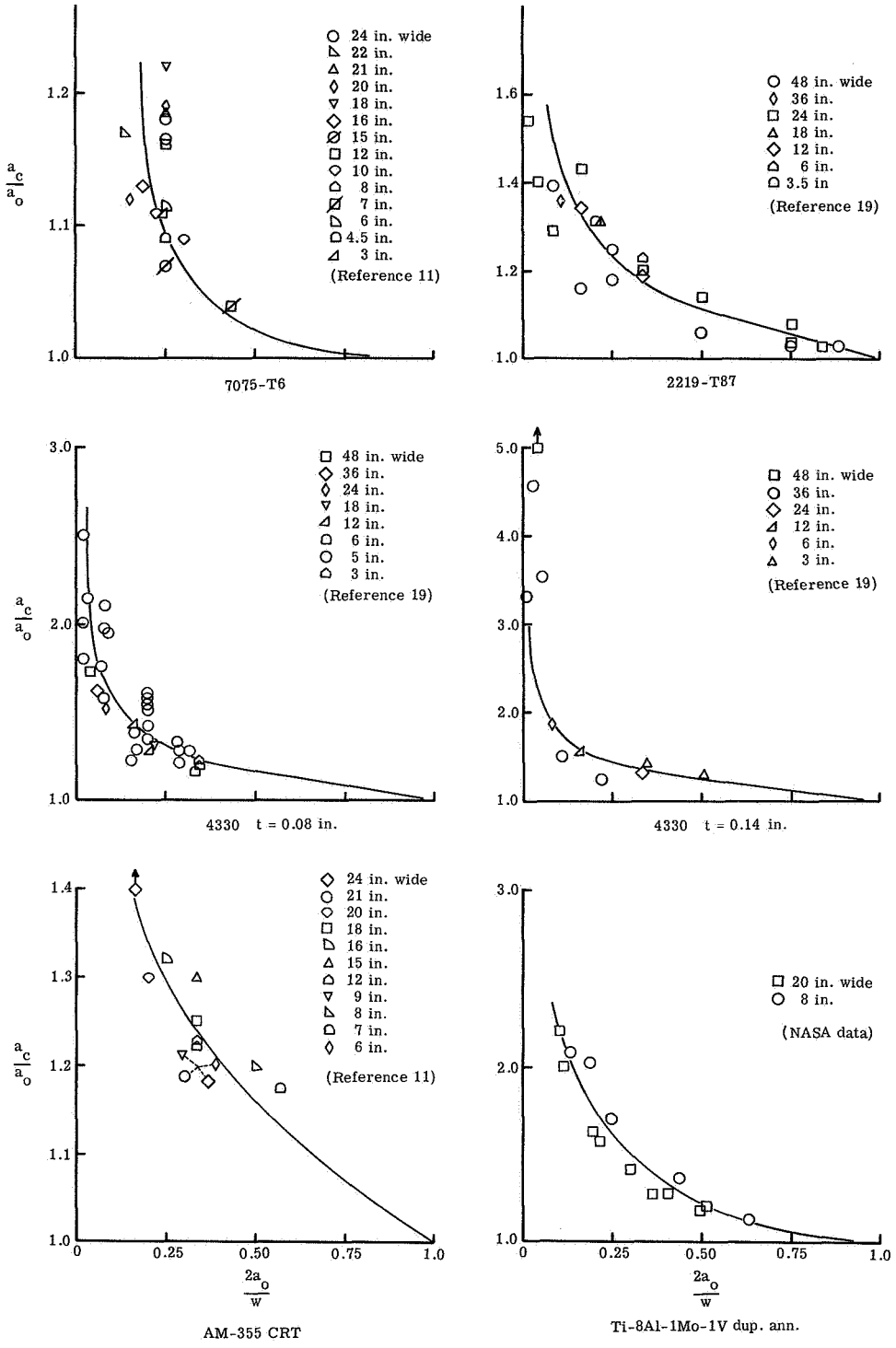

Figure 5.- Ratio of critical-to-initial crack length as a function of initial crack length-to-width ratio. The curves represent equation (14).

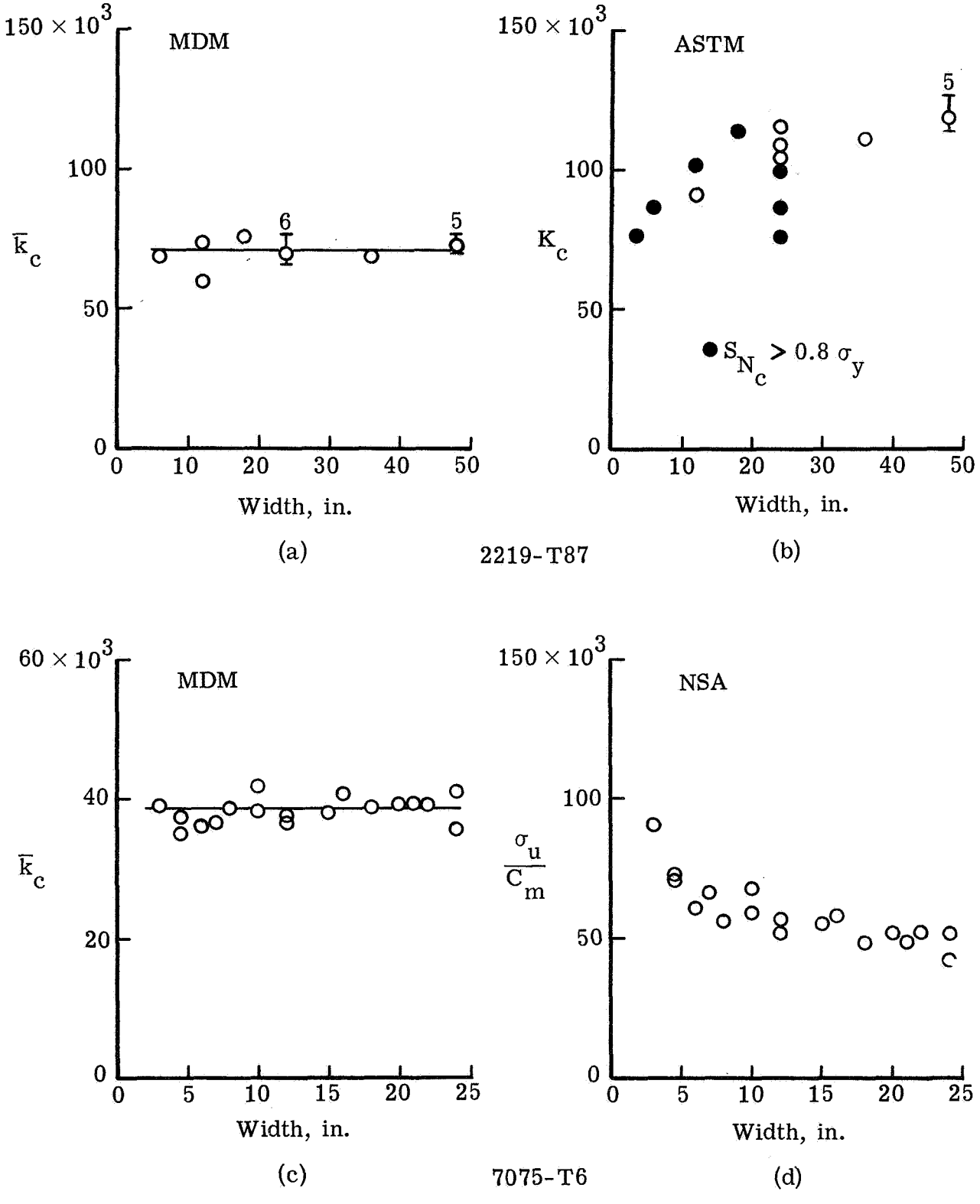

Figure 6.- Fracture toughness or crack sensitivity plotted as a function of width.

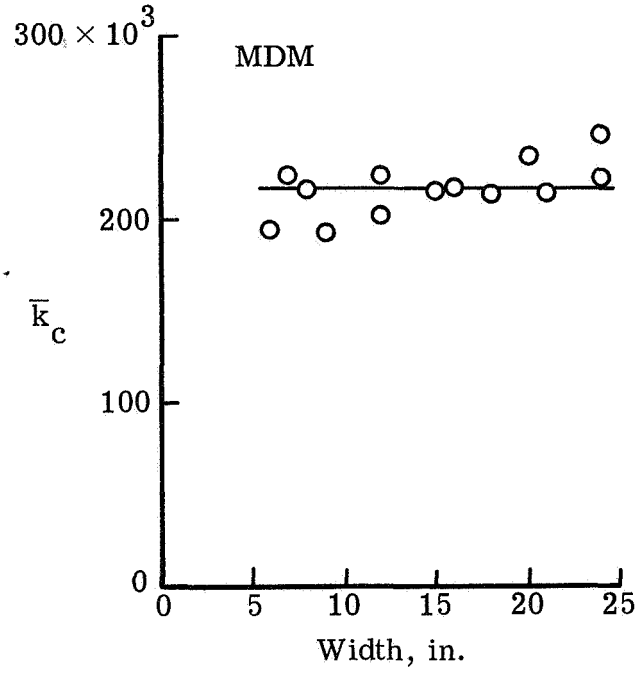

(e) AM-355 CRT

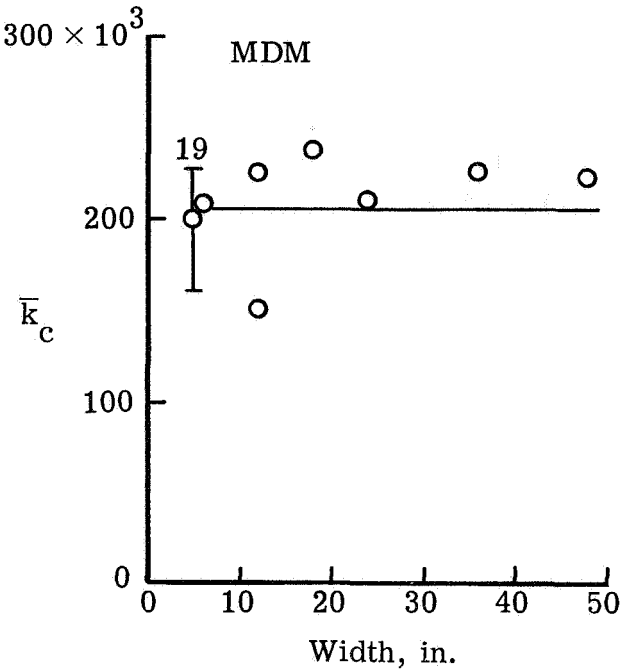

(f) 4330 t = 0.08 in.

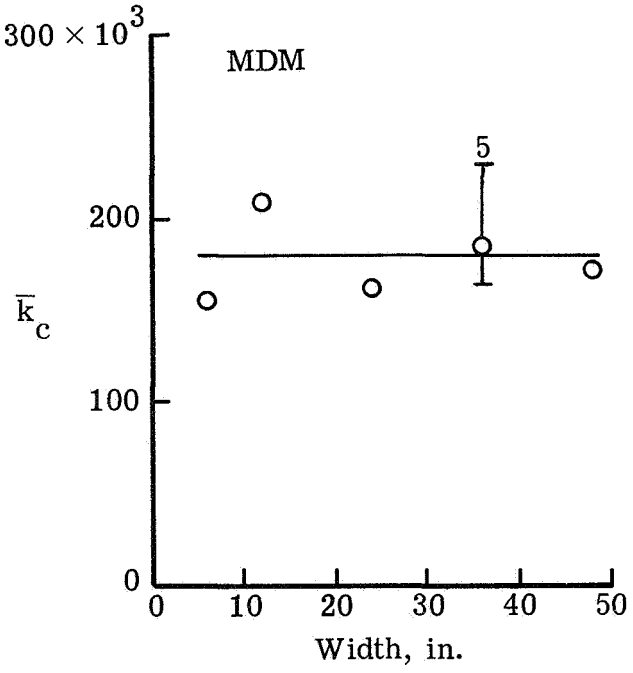

(g) 4330 t = 0.14 in.

Figure 6.- Concluded.

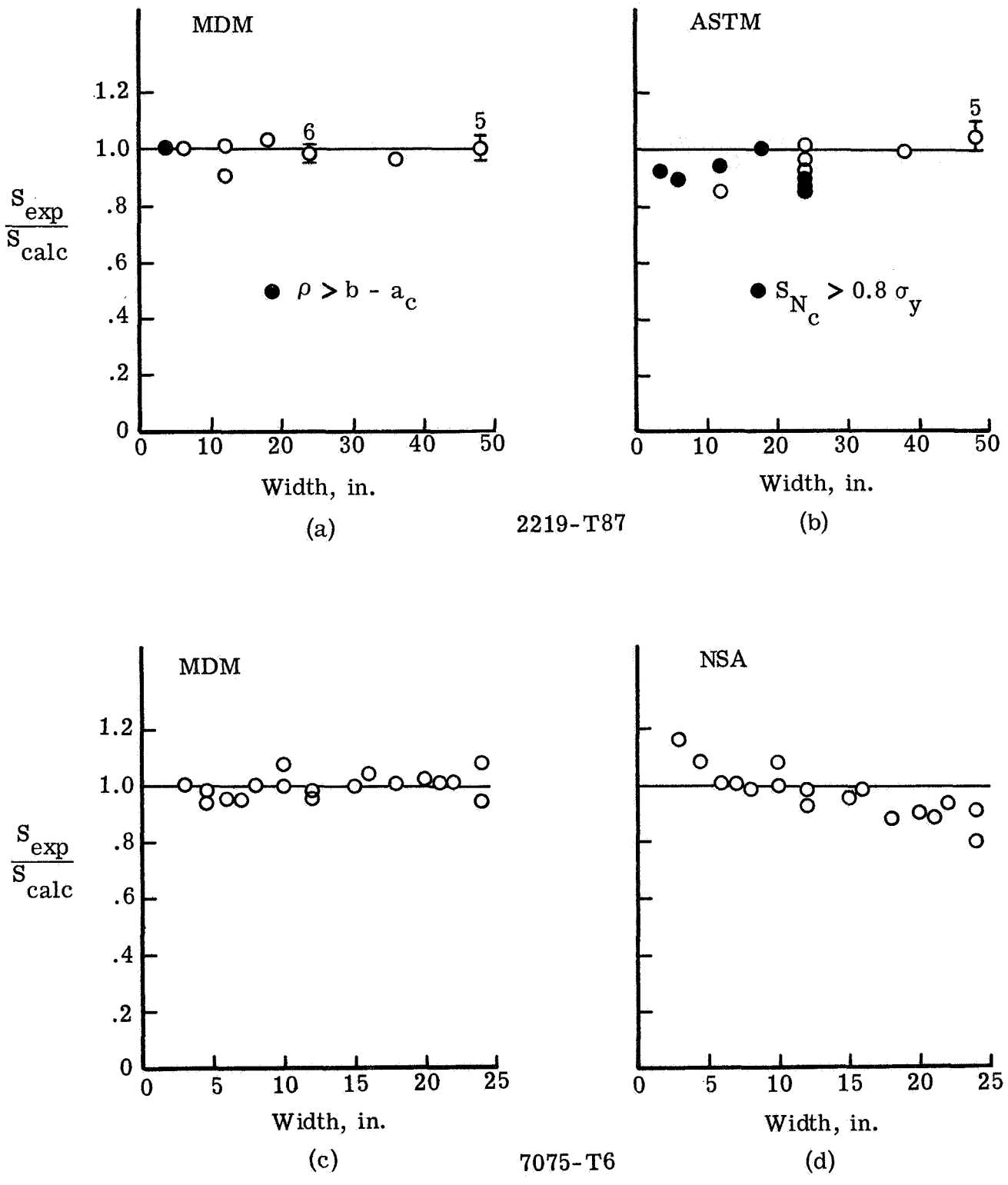

Figure 7.- Ratio of experimental to calculated gross stress plotted as a function of panel width.

NASA-Langley, 1967